Chapter 5
New Developments in a 1D+ ISM Model for Operational Purposes

Yassine Kaddi, François-Xavier Cierco, Jean-Baptiste Faure, and Sébastien Proust

Abstract In order to provide realistic and fast predictions of water level and flow partition across an overflowing river, Proust et al. (Water Resour Res 45:1–16, 2009) developed the 1D + Independent Subsection Model (ISM) in order to better represent the mass balance between the river main channel and the adjacent floodplains. This model was proved to perform better than other 1D models in different benchmarks in laboratory flumes [5], [13], [27] particularly to predict water depths and discharges per subsection in the floodplain for steady flows in both uniform and non-uniform conditions. Nevertheless, at the time, ISM was not suited for operational purposes. Therefore, additional developments were achieved so as to (i) enable ISM to simulate unsteady flows, (ii) derive and set relevant boundary conditions from routine data by partitioning the inflow discharge between main channel and floodplains, (iii) solve the mass balance equation for any subsection in river junctions. These developments were implemented in the research code MAGE, developed by INRAE to model open channel flows under subcritical conditions. New 1D + simulations were thus run and compared to experimental data collected either in a laboratory flume under unsteady overbank flow conditions, or in the fields for overbank flows in steady conditions.

Y. Kaddi (✉) · J.-B. Faure · S. Proust
INRAE, CS 20244, 69625, 5, Rue de la Doua, 69100 Villeurbanne, France
e-mail: yassine.kaddi@inrae.fr

J.-B. Faure
e-mail: jean-baptiste.faure@inrae.fr

S. Proust
e-mail: sebastien.proust@inrae.fr

F.-X. Cierco
C.N.R., Direction de l'ingénierie et des grands projets, 2, Rue André Bonin, 69004 Lyon, France
e-mail: f.cierco@cnr.tm.fr

P. Gourbesville and G. Caignaert (eds.), *Advances in Hydroinformatics*, Springer Water,
https://doi.org/10.1007/978-981-19-1600-7_5

This paper reports the preliminary numerical tests as well as cross-comparisons with other 1D codes against the specific dataset described above.

Keywords Overbank flows · Unsteady flows · Head loss · Inflow discharge partition · Laboratory experiment · Field data

5.1 Introduction

1-D simulations offer several advantages in order to provide realistic predictions of water levels in operational conditions such as for flood or energy production management. As an example, they can be run and calibrated with routine data collected in the fields, whereas 2-D and 3-D models generally request extra information and specific measurement campaigns. Moreover, their short computation times and robustness make 1-D simulations well suited for real-time assessments and crisis management. Although local discrepancies are often noticed between numerical predictions and observed data, the delivered results are solid enough for the purposes of interest. Nonetheless, the observed gaps may be more important when the flow conditions get far from the 1-D modelling assumptions (e.g. for slightly overbank flows, or in confluences or diffluences).

Despite the proven capabilities of 1D models, the local gaps between predictions and observations for overbank flows should be questioned as they result in uncertainties in threshold discharges or arrival time of the surge in floodplains, where different vulnerabilities may be present (housing, public equipment…). Most of classical 1D models rely on the Divided Channel method, DCM, [6], and on the Manning–Strickler bed friction law to close the momentum budget. Ervine et al. [7] pointed out the fragile modelling of head losses in such models. Considering that the dissipation terms may be influenced by turbulent and momentum exchanges between main channel and floodplains in addition to bed friction, Bousmar et Zech, [2], proposed an additional term in the momentum equation and built the Exchange Discharge Model, EDM. Such modelling relies on the concept of the apparent shear stress at the interface between subsections. Several propositions were made to derive the apparent shear stress resulting in the Apparent Shear Stress Model, ASFM, from Moreta and Martin-Vide [14] or in the Interacting Divided Channel Method, IDCM detailed by Huthoff et al. [9].

Because the main hypothesis of 1D models is to consider averaged flow parameters across the total wet cross-section, 1D modeling does not enable to re-discretize discharge or flow velocity per subsection without additional assumptions, sometimes violating the mass conservation equation or the Manning–Strickler friction law (see [27]). Nevertheless, early advanced formulations of the DCM attempted to overcome this limitation such as the DEBORD formulation (Nicollet and Uan [15]) or other so-called corrected DCM as Ackers' coherence method (Ackers [1]). Nevertheless, discussions are still running on the proper definition (and thus, the proper delimitations) of compound bed subsections, since several criteria may be equally relevant.

Lambert et Myers, [12], attempted to overcome that difficulty through the weighted divided channel method (WDCM), which combines different divisions of the channel (for a revue, see Fernandes et al. [8] and Bousmar et al. [5]).

Nevertheless, investigations of the structure of the flow at the interface between the floodplain and the main channel proved that extra phenomena such as mass and momentum transfers occur between subsections. These latter are largely involved in the global dynamic of overbank flows; they influence the discharge distribution in the subsections as well as the water level in the floodplain (e.g., Bousmar et al. [3], Peltier et al. [16], Proust et al. [17, 20, 21]). Different efforts were conducted to model the effects of those interactions, resulting in the Interacting Divided Channel Method, IDCM, (Huthoff et al. [9]) in the Independent Sub-section Method, ISM, (Proust et al. [18, 19]). The latter solves a unique mass conservation equation on the total cross-section as well as a momentum conservation equation in each of the subsection (main channel, left-hand and right-hand floodplains). Despite promising results were obtained in laboratory flumes ([5, 13, 27]), the ISM has never been validated against field data due to its lack of adaptability to operational situations and real river flows.

Therefore, recent improvements were achieved in the ISM solver in order to enable unsteady flow computations. The performances of the new solver were evaluated against experimental data collected in an asymmetric compound open-channel flume for different flow configurations under unsteady conditions (as described in Kaddi et al. [10]). The flow partition between main channel and floodplain set as upstream boundary condition was also questioned since ISM requests one inflow discharge in each subsection, whereas routine data only provide the discharge across the total river cross-section. To that purpose, the uncertainty propagation due to an erroneous upstream flow partition was investigated as well as a new method to derive the discharge in each subsection. The mass conservation equation was also locally modified to be suitable for the merging of two compound channel flows in a confluence, in which the internal floodplains necessarily disappear. Last, the improved ISM model was evaluated on a field test-case, namely, the upstream part of the Bourg-Lès-Valence reservoir, on the Rhône river, and cross-compared with one DCM-model and one corrected DCM model.

5.2 Validation of ISM Under Unsteady Conditions

Since overbank flows occur during discharge peaks whose length may range from tens of hours to several weeks, one of the challenging parts of this work consisted in modifying the ISM solver previously implemented in MAGE in order to enable computations under unsteady conditions. As detailed below, the ISM modelling ([10, 18]) relies on a description of the river as a compound open channel, which primarily consists of at least one main channel (MC) and two lateral floodplains (FPs) including one left-hand FP and one right-hand FP.

In what follows, a "depth uniform" flow or an "equivalent uniform flow" must be understand as an experimental flow for which no change occurs in water depth along the flume although variations are expected in the spatial velocity distribution due to the bed geometry. In such flows, the discharge distribution in MC and FCs is expected to be close to the discharge distribution derived by the DEBORD Formula (see [15]). Another formulation will also be proposed in § 5.3.1.1.

5.2.1 ISM Formulation Under Unsteady Flow Conditions

The ISM solves a set of four coupled ordinary differential equations: one mass conservation equation across the total cross-section (Eq. 5.1), and three momentum conservation equations (one in each of subsection). The momentum equation in the MC is written in Eq. (5.2) and in each of the two FCs, in Eq. (5.3):

$$\frac{\partial A}{\partial t} + \frac{\partial (Q_m + Q_f)}{\partial x} = 0 \tag{5.1}$$

$$\frac{\partial Q_m}{\partial t} + \frac{\partial}{\partial x}\left(\frac{Q_m^2}{S_m}\right) + gA_m\frac{\partial Z}{\partial x} = -gA_m J_m - \frac{\tau_{\text{int}} h_f}{\rho} + U_{\text{int}} q \tag{5.2}$$

$$\frac{\partial Q_f}{\partial t} + \frac{\partial}{\partial x}\left(\frac{Q_f^2}{S_f}\right) + gA_f\frac{\partial Z}{\partial x} = -gA_f J_f + -\frac{\tau_{\text{int}} h_f}{\rho} + U_{\text{int}} q \tag{5.3}$$

where A refers to the total wet cross-section area, Z, the water surface elevation with respect to a reference datum, q, the lateral discharge per unit length (positive with a flow from MC to FP) as defined below in Eq. 5.4, A_i, the wet area of subsection i, J_i, the head loss gradient in subsection i, h_i, the flow depth in subsection i, with i = m or f in MC or FP, respectively. U_{int} stands for the depth-averaged streamwise velocity and τ_{int} is the depth-averaged transverse Reynolds shear stress at the MC/FP interface. The discharges in MC and FP, are denoted as Q_m and Q_f, respectively.

$$q = \frac{\partial A_f}{\partial t} + \frac{\partial Q_f}{\partial x} \tag{5.4}$$

In the following, U_{int} is derived from the subsection-averaged velocities U_m and U_f, like in the case of non-prismatic channels ([19]):

$$U_{\text{int}} = \phi U_m + (1 - \phi) U_f \tag{5.5}$$

where ϕ is a weighting coefficient.

The interfacial Reynolds shear stress τ_{int} is derived from a mixing length model following Bousmar et Zech, [2], and the formulation of the Exchange Discharge

Model (EDM):

$$\tau_{\text{int}} = \rho \psi^t \left(U_m - U_f\right)^2 \tag{5.6}$$

where ψ^t is a turbulent exchange coefficient whose recommended value equals 0.16 in the EDM ([2]) that solves the momentum equation on the total cross-section, and equals 0.02 in the ISM ([18]).

It should be noted that the set of Eqs. 5.1–5.3 is entirely based on the subsection discharges Q_m and Q_f without any reference to the total discharge. As a result, the solver has to consider three independent discharges instead of one as upstream boundary conditions. This point will be addressed in part 5.3.1.

5.2.2 Solver Modifications in Code MAGE

ISM has been implemented in an operational numerical code, MAGE, developed by INRAE, previously designed for solving the shallow water equations in compound channels based on a corrected DCM, termed the DEBORD method. The ISM has thus been implemented by taking advantage of the pre-existing structure of MAGE. As a result, MAGE-ISM is based on a Preissmann numerical scheme (i.e. semi-implicit difference scheme). Since the modifications in the set of equations do not affect their nature but only their number (4 rather than 2), the solver remains unchanged and still uses the simplified Newton–Raphson iterative method. Nevertheless, the resolution procedure has been re-written to take advantage of the block tridiagonal structure of the linear system. Nowadays, MAGE may be run using either the ISM or the DEBORD method. It should be noted than ISM accounts for the left-hand and right-hand FPs as independent subsections, whereas only one global FP is considered with the DEBORD method.

Last, the solver has been modified to consider in the upstream boundary condition the three inflow sub-section discharges (in the ISM) while the DEBORD method only requests the total inflow discharge. As routine data only provide the total inflow discharge Q, specific modules were implemented to disaggregate the Q-value in the discharges Q_m and Q_f. To that purpose, several methods were proposed, namely: (i) iteratively compute the discharge distribution by initializing the computation with an arbitrary discharge distribution before reporting back the one computed in the second cross-section at the previous time-step; (ii) computing the "equivalent uniform distribution" in steady conditions derived from the DEBORD formula (see [15]) and (iii) computing the ISM "equivalent uniform steady distribution" computed using Eqs. 5.9–5.12 (see § 3.1).

The procedure ensuring mass balance in compound channel junctions is not detailed here since the method validation is still running. It should be noted that the transition from dry to wet floodplains is not addressed in the present state of ISM developments, these latter ensuring the solving of ISM equations over completely

wet floodplains only. This difficulty is related to the implicit scheme used for the solving of the set of Eqs. (1)–(3) derived from the Shallow Water Equations.

5.2.3 Validation Against Laboratory Data

The implementation of the set of equations previously mentioned in § 2.1 was validated against experimental data collected in a compound channel flume located at INRAE Lyon, France.

5.2.3.1 Experimental Setting

The compound channel flume has an asymmetric cross-section composed of a MC and a left-hand FP (see Fig. 5.1). The MC and FP are supplied with water independently (two independent tanks and pumps), allowing the setting of the inflow partition between MC and FP at the flume entrance. The experimental facility is detailed in [10].

In that experiment, two unsteady flow cases were studied denoted as Flow 1 and Flow 2, which differ by their upstream flow partition between MC & FP at any time t. For each of the flow cases, the inlet hydrograph was repeated 100 times corresponding to 100 bursts or peak flows (with discharge Q^p) departing from a common base flow (initial and final discharge Q^b). A dedicated windowing technique was then applied to the time series made of the 100 hydrograph repetitions (see [10]). The main characteristics of the two streams were therefore derived as an ensemble average computed from the 100 individual hydrographs. Namely, for a given variable of

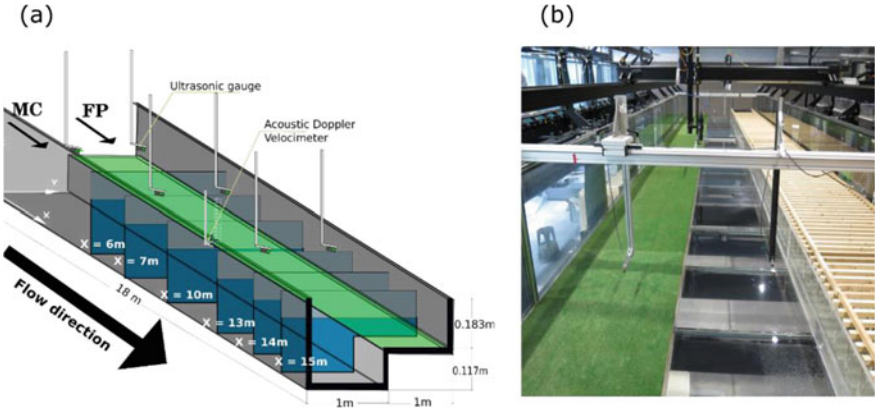

Fig. 5.1 (a) Sketch of the compound channel flume located at INRAE Lyon, France, (b) Photograph of the flume looking downtream

interest, P(t), characterizing either Flow 1 or Flow 2:

$$\langle P \rangle(t) = \frac{1}{100} \sum_{i=1}^{100} P_i(t) \tag{5.7}$$

where i refers to the number of the single windowed hydrograph.

The ensemble-average < Q > (t) and the standard deviation σ_Q (t) of the total inflow discharge as a function of time x is depicted in Fig. 5.2 for flow 1. Higher values of σ_Q can be observed during the rising and falling limbs. Nevertheless, <Q> (t) was proved to converge with a relatively good accuracy of $\pm 0.2\,\mathrm{Ls}^{-1}$ after 60 runs in both FP and MC. Similar results were obtained for the flow depth in the FP < h_f > (t) at X = 6 m. The flow depth standard deviation was found of the same order of magnitude as the fluctuations of the instantaneous measurements of flow depth (~4 mm).

The averaged features of the two flows case are summarized in Tables 5.1 and 5.2. Table 5.1 focuses on the ensemble-averaged discharges in each subsection and provides the rising and decreasing limb duration (T_Q^r and T_Q^d respectively), as well as the total duration of the surge (T_Q). Table 5.2 displays the ensemble-averaged water depths in the MC and FP, the water depth ratio and the unsteadiness flow parameter, λ, defined in Eq. 5.8 following Takahashi et al. [24] and Tominaga et al. [26]:

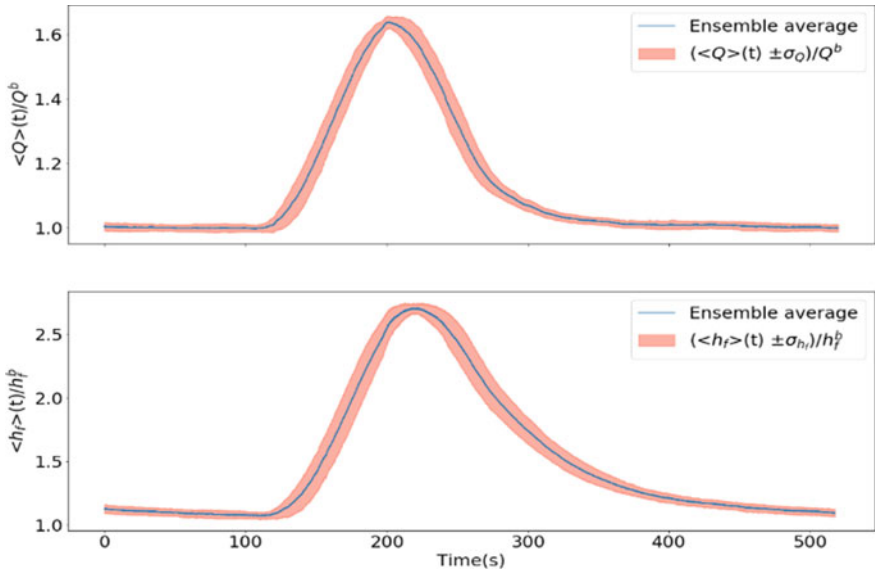

Fig. 5.2 Inlet total discharge < Q > normalized by the baseflow total discharge Q^b (top). Water depth in the FP, h_f, normalized by the baseflow FP water depth, $h^b{}_f$ at X = 6 m (bottom)

Table 5.1 Main features of the inlet hydrographs at the flume entrance for cases Flow 1 and Flow 2

		$Q\ (L.s^{-1})$	$Q_m\ (L.s^{-1})$	$Q_f\ (L.s^{-1})$	$Q_f/Q\ (\%)$	$T_Q^r\ (s)$	$T_Q^d\ (s)$	$T_Q(s)$
Flow 1	Base flow	101	94	7	7	90	170	520
	Peak flow	166	140	26	16			
Flow 2	Base flow	110	99	10	10	150	230	550
	Peak flow	192	138	28	28			

Table 5.2 Main features of the water depth time series measured at X = 10 m. for Flow 1 and Flow 2

		$h_m\ (mm)$	$h_f\ (mm)$	$h_r = h_f/h_m$	$T_h^r\ (s)$	$T_h^d\ (s)$	λ_m	λ_f
Flow 1	Base flow	135.6	21.4	0.16	105	275	0.22	0.37
	Peak flow	166.0	50.4	0.30				
Flow 2	Base flow	145.4	29.1	0.20	150	250	0.19	0.32
	Peak flow	186.6	70.7	0.38				

$$\lambda = \frac{\langle h^p \rangle - \langle h^b \rangle}{S_o T_h^r \sqrt{g < h^p >}} \tag{5.8}$$

where $< h^p >$ and $< h^b >$ refer to the ensemble-averaged flow depth at peak flow and at base flow, respectively. T_h^r and T_h^d stand for the rising and decreasing limb duration respectively. T_Q is the duration of a single hydrograph after windowing. It includes a long enough time lapse of the steady base flow before and after the rising and falling limbs respectively. S_0, stands for the flume slope. It should be noted that the unsteadiness flow parameter, λ, was defined independently in each subsection.

Flow 1 and Flow 2 slightly differ by their dynamics as it can be appreciated thanks to the unsteadiness flow parameter λ. In both cases, the λ-values are relatively small compared to those reported in the literature. For example, they ranged from 0.19 to 0.75 in Tominaga et al. [25], or from 0.38 to 5.03 in Lai et al. [11]. The specificities of Flow 1 and Flow 2 are shown in Fig. 5.3, which compares the measured discharges upstream of the MC and FP thanks to the theoretical discharge partition of the "equivalent uniform steady flow" of same total cross-section wetted area derived from the DEBORD formula, [15]. Flow 1 was designed to be close to the theoretical discharge partition of a succession of "equivalent uniform steady flows" at any time t, whereas Flow 2 is further from equilibrium with a significant excess in FP flow along the whole hydrograph. The difference in the upstream flow partition between MC and FP is visible in Fig. 5.3.

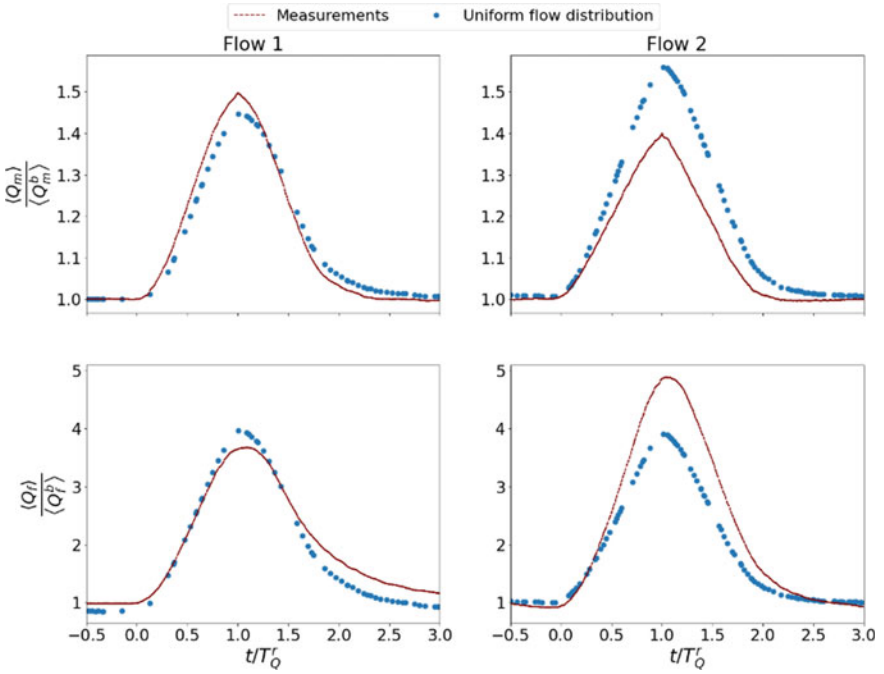

Fig. 5.3 Inlet instantaneous discharge normalized by the subsection baseflow discharge in MC (top) and in FP (bottom)

5.2.3.2 Validation of the ISM Under Unsteady Flow Conditions

As stated in § 5.2.1 and 5.2.2, ISM was redeveloped and implemented in the 1D numerical code MAGE to be suitable for unsteady flows and actual river geometries. Interestingly, ISM specificities allow detailing the results per subsection, as well as computing extra variables that describe the mass transfer from the main channel to the floodplain, or the momentum exchange between MC and FP. As a result, either the ensemble-averaged flow depth in the floodplain, $< h_f >$, or additional interfacial variables such as the depth-averaged streamwise velocity $< U_x >_d$, corresponding to U_{int} in ISM equations (Eqs. 5.1–5.3), the transverse velocity, $< U_y >_d$ (=q/h_f), and the lateral discharge, q, (defined in Eq. 5.4), can be simulated at the MC/FP interface. The simulations hereafter were run with $\Phi = 0.3$ and $\psi^t = 0.02$ in Eq. 5.5 and Eq. 5.6 respectively. The results are plotted against the experimental measurements detailed in § 5.2.3.1 as well as against simulations using the DEBORD model when available in Figs. 5.4 and 5.5.

Although both modelling techniques (1D DEBORD and 1D + ISM) perform equally to simulate unsteady flows characterized by an upstream discharge partition between MC and FP close to equilibrium at any time t, ISM provides better results for significantly unbalanced discharge distributions (Fig. 5.4). Interestingly, the time

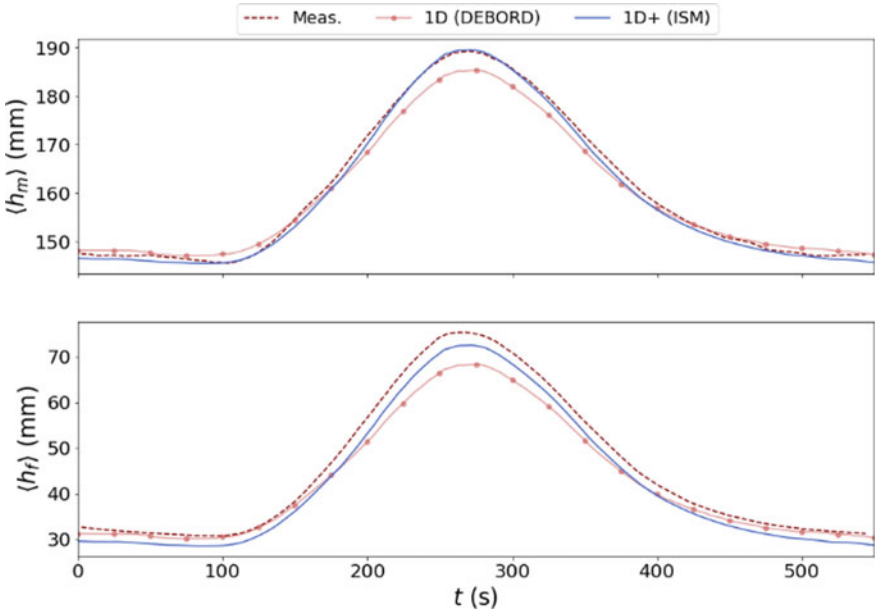

Fig. 5.4 Measured and simulated flow depth in MC $< h_m >$ (top) and FP $< h_f >$ (bottom) for case Flow 2 at X = 6 m

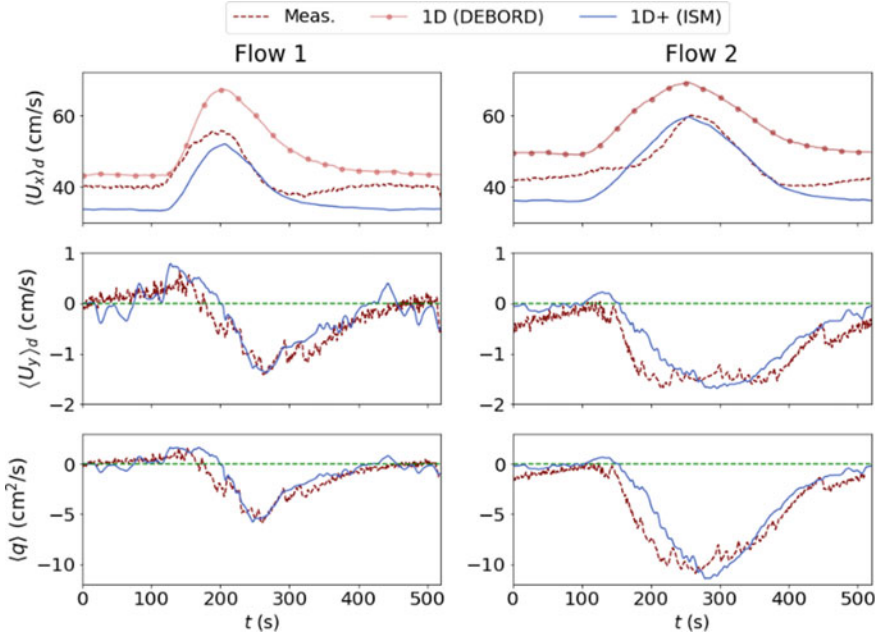

Fig. 5.5 Measured and simulated depth-averaged streamwise velocity $< U_x >_d$, transverse velocity $< U_y >_d$, and lateral discharge q at the MC/FP interface at X = 10 m

evolution and the sign of both $< U_y >_d$ and the lateral discharge, q, are well captured by the model (see Fig. 5.5) either for Flow 1 or Flow 2. The relative error in the simulated evolution of $< U_x >_d$ is considerably better with ISM than with DCM-DEBORD: for Flow 1, it reaches a quite acceptable mean of 6% with ISM (vs 15.6% with DCM-DEBORD) and does not exceed 14% (vs 36.23% with DCM-DEBORD). For Flow 2, the mean relative error is 8.8% (vs 20% with DCM-DEBORD) and the maximum relative error rises 24.5% (vs 33.6% with DCM-DEBORD).

The ISM ability to provide both the main longitudinal and lateral flow velocities allow investigating the hysteresis response of the water depth to the discharge surge commonly observed in unsteady flows. In other terms, the main velocity of the flow is not a bijective function of the water depth but varies differently depending on the flow dynamics, namely during the rising or falling limbs. The simulations performed with ISM are compared to the experimental measurements in Fig. 5.6. Interestingly, the global shape of the hysteresis response of the flow is well captured by the ISM simulations for both test cases (the quality of the results is quite similar for Flow 1 and Flow 2). All these results are very promising and prove the abilities of the new ISM algorithm to provide satisfactory simulations under unsteady flow conditions.

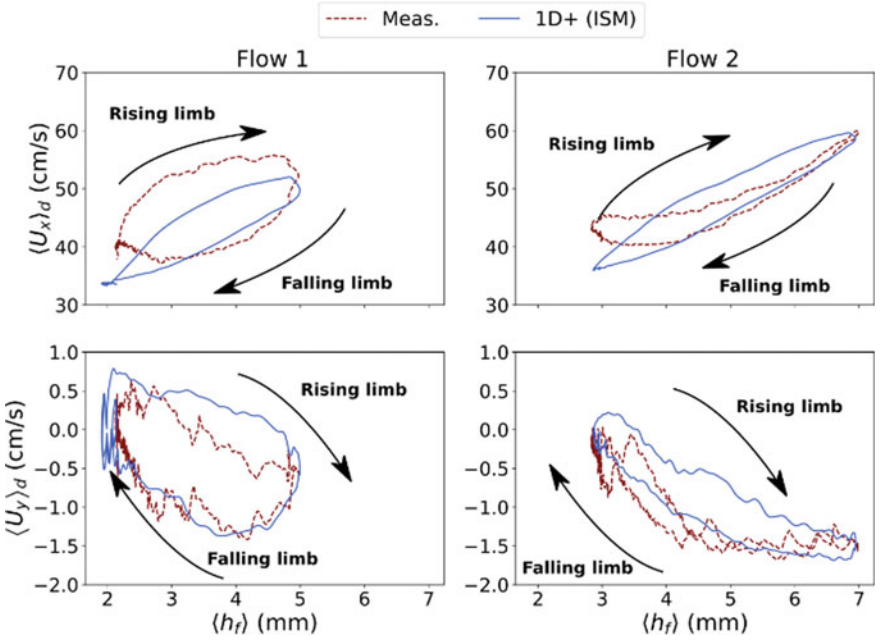

Fig. 5.6 Depth-averaged streamwise velocity and transverse velocity at the MC/FP interface as a function of the FP flow depth showing hysteresis loops: simulated results (blue plain line) versus measurements (detached red line)

5.3 Further Developpements for Operational Purposes

5.3.1 Derivation of Well-Suited Boundary Conditions

As stated in § 2.1, the ISM solver requests adapted upstream boundary conditions, namely the inflow discharge in the MC, Qm (x = 0), and the two inflow discharges in the left-hand and right-hand FPs, denoted as Q_l (x = 0) and Q_r (x = 0), respectively. Unfortunately, routine data only provide the global discharge averaged across the total river cross-section, Q. Therefore, a new method for partitioning the Q-value at x = 0 into values of Qm, Ql and Qr was developed and evaluated. In addition, a sensitivity analysis was conducted to estimate the impact of the initial discharge partition on the streamwise evolution of the flow.

5.3.1.1 Derivation of the Discharge Partition from the ISM Equations for a Uniform Flow

Two solutions were investigated in order to derive a well-suited inflow discharge partition between MC and FP as upstream boundary condition for ISM models: (i) by applying the DEBORD Formula ([15]) or (ii) by solving the ISM equation under steady uniform flow conditions. Method (ii) is expected to provide more consistent results for an ISM model, whereas method (i) may be consider as the up-to-date reference. Both proposed methods are designed to deliver the discharge partition of the "equivalent uniform flow (of same wetted area)" and should thus be challenged for various flow conditions, including unbalanced upstream flow partitions.

Practically, method (ii) consists in solving the set of Eqs. 5.9–5.12, assuming that the total discharge Q and the turbulent exchange coefficient ψ^t were previously estimated:

$$Q - U_r A_r - U_m A_m - U_l A_l = 0 \tag{5.9}$$

$$S_o - \frac{U_r^2}{K_r^2 R_r^{4/3}} + \psi^t \frac{h_r (U_m - U_r)^2}{g A_r} = 0 \tag{5.10}$$

$$S_o - \frac{U_m^2}{K_m^2 R_m^{4/3}} - \psi^t \frac{h_r (U_m - U_r)^2 + h_l (U_m - U_l)^2}{g A_m} = 0 \tag{5.11}$$

$$S_o - \frac{U_l^2}{K_l^2 R_l^{4/3}} + \psi^t \frac{h_l (U_m - U_l)^2}{g A_l} = 0 \tag{5.12}$$

The four variables h_f, (with $h_f = h_l = h_r$), U_m, U_r, and U_l may thus be derived of the previous set of equations (with R_m and R_f the hydraulic radius in MC and right-hand FP respectively):

5.3.1.2 Validation Against Experimental Data

The impact of the upstream flow partition was primarily validated against steady "depth-uniform" and "depth-non-uniform" flows in a compound channel (Proust et Nikora, [22]), for which the MC/FP flow partition can be far from equilibrium. The inflow discharge partition methods were also tested against unsteady flows using the test cases Flow 1 and Flow 2 previously described in § 2.3. For both steady and unsteady flows, the ISM was run with three different upstream flow partitions: (i) the partition of the "equivalent uniform flow of same wetted area" derived from the DEBORD formula and denoted here as Rep-D; (ii) the ISM "equivalent uniform distribution" computed using Eqs. 5.9–5.12 (Rep-Unif); and (iii) the actual measured flow partition at the entrance of the flume (Rep-Exp). The results of those simulations were then compared to the measured data (Meas.).

The simulations of the steady depth-uniform flow studied by Proust and Nikora, [22], are shown in Fig. 5.7, and the simulations of the unsteady cases (Flow 1 and Flow 2, see § 5.2.3) in Fig. 5.8 and Fig. 5.9. For the "equivalent uniform flows" (e.g. in Fig. 5.7 as well as for Flow 1 in Fig. 5.8 and Fig. 5.9), the second option (ii =

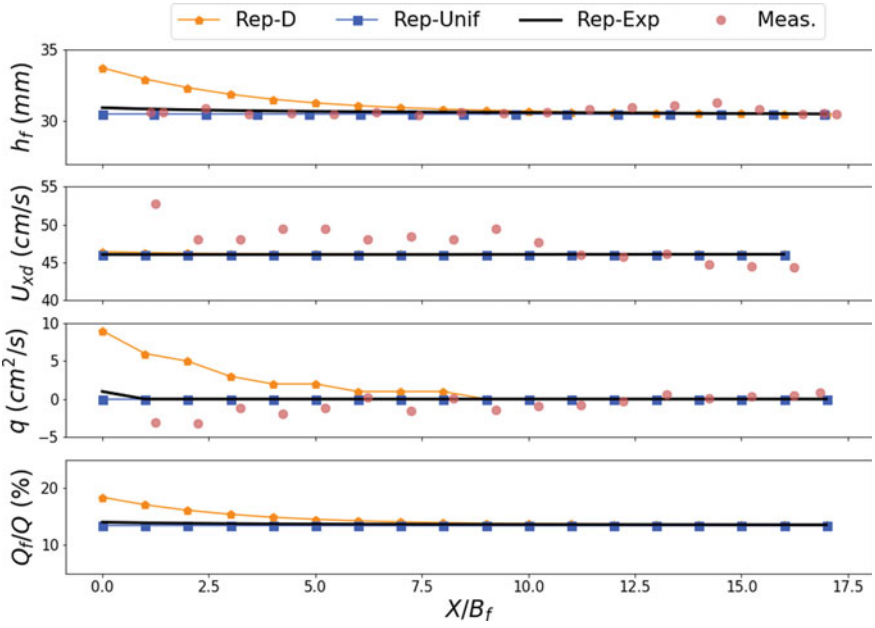

Fig. 5.7 Longitudinal profile of 4 variables of interest simulated by ISM with three different inlet discharge distributions plotted against experimental measurements (when available) of a depth-uniform flow (Proust and Nikora [22]). The experimental values are indicated by pink circle markers whereas the orange, blue and black solid lines represent the three different discharge partitioning imposed at the flume entrance: the DEBORD uniform distribution (Rep-D), ISM uniform distribution (Rep-Unif) and experimental distribution (Rep-Exp) respectively. B_f stands for the channel floodplain width

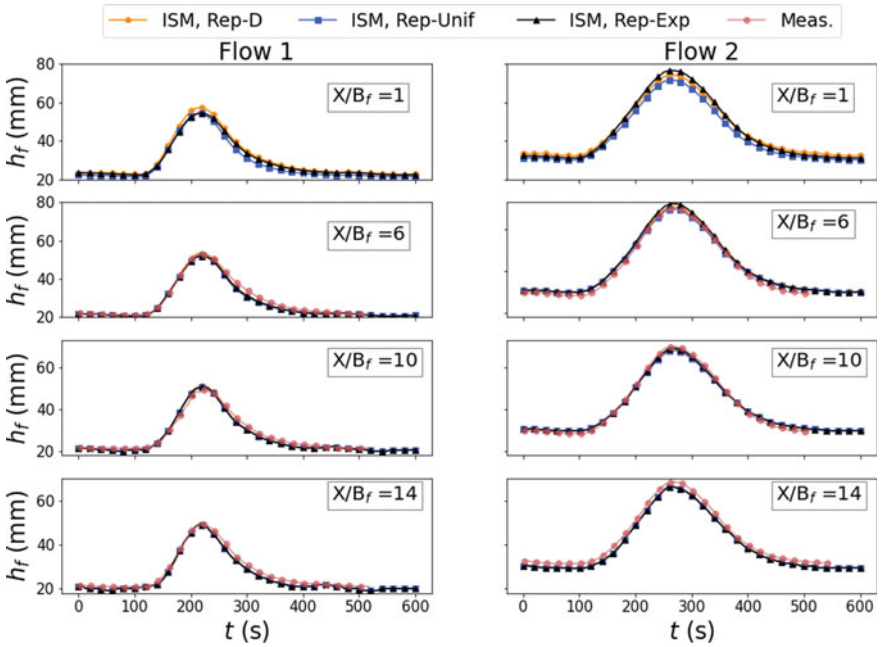

Fig. 5.8 Water depth time series in the FP for Flow 1 (left) and Flow 2 (right) for various longitudinal positions along the flume. The different simulations were obtained with upstream boundary conditions obtained similarly as in Fig. 5.7. B_f stands for the channel floodplain width

ISM discharge distribution = Rep-Unif) provides very good estimates of flow depth h_f. The results for the lateral discharge, q, are also better than those provided by the Debord method (Rep-D).

Furthermore, results obtained with option ii (Rep-Unif) are comparable with those of option iii (Rep-Exp) for all investigated variables. In every case, the Debord distribution (option i, Rep-D) results in more questionable simulations in the upper part of the flume, particularly for distances less than $X/B_f < 10$, with B_f, denoting the FP width.

As Flow 1 is closer to equilibrium i.e. to the "equivalent uniform flow", smaller discrepancy was expected in the simulation results for Flow 1 than for Flow 2 irrespective of the boundary conditions (namely options i, Rep-D, ii, Rep-Unif and iii, Rep-Exp). This prediction is confirmed at $X/B_f = 1$ for the water level (Fig. 5.8) and the discharge ratio (Fig. 5.9). The effects of the boundary conditions are restricted to the upstream part of the stream, since no impact of the boundary conditions nor in the water depth neither in the discharge ratio could be noticed downstream of $X/B_f = 14$. As expected, the simulations converge faster for Flow 1 ($X/B_f = 6$ for water depth, $X/B_f = 10$ for discharge ratio) than for Flow 2 ($X/B_f = 10$ and 14, respectively). Discrepancy also collapses faster for water depth than for discharge ratio. The adimensional distance before the simulated flow returns to the uniform state was also proven to be less than 15 in the depth-non-uniform flows of Proust and

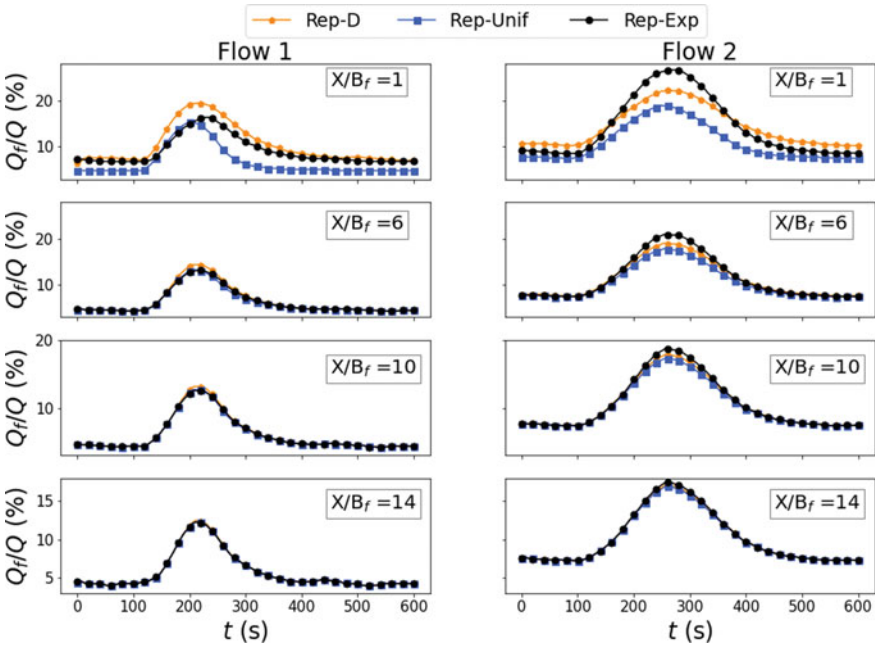

Fig. 5.9 Discharge distribution time series in the floodplain for Flow 1 (left) and Flow 2 (right) for various longitudinal positions along the flume

Nikora [22]. This latter result was obtained for every following variable of interest: h_f, q, Q_f/Q, supporting the conclusions of Bousmar et al. [4], who stated that the flow returns to uniform conditions in the range $X/B_f = 8$ to 35.

This first conclusion was confirmed by the results of a sensitivity analysis. These latter investigated a larger range of boundary conditions. Therefore, the inlet discharge partition was arbitrarily modified so that the proportion of the floodplain discharge ranged from – 50% up to 120% compared to the expected "uniform distribution" in the experimental case of Sect. 2.1. To that purpose, the upper part of the flume model was extended in order to get enough length available. The results confirm once again the conclusions of Bousmar et al. [4], as displayed in Fig. 5.10.

5.4 ISM Validation Against Field Data

The Bourg-Lès-Valence reservoir is part of the Rhône river, France. It was chosen as a case study in order to benchmark ISM modelling in operational conditions. This benchmark consisted in simulations run over the upper part of the reservoir called "Vieux-Rhône". The studied reach is located downstream of the Arras dam (Fig. 5.11) so that the upstream boundary condition is perfectly well-known. There

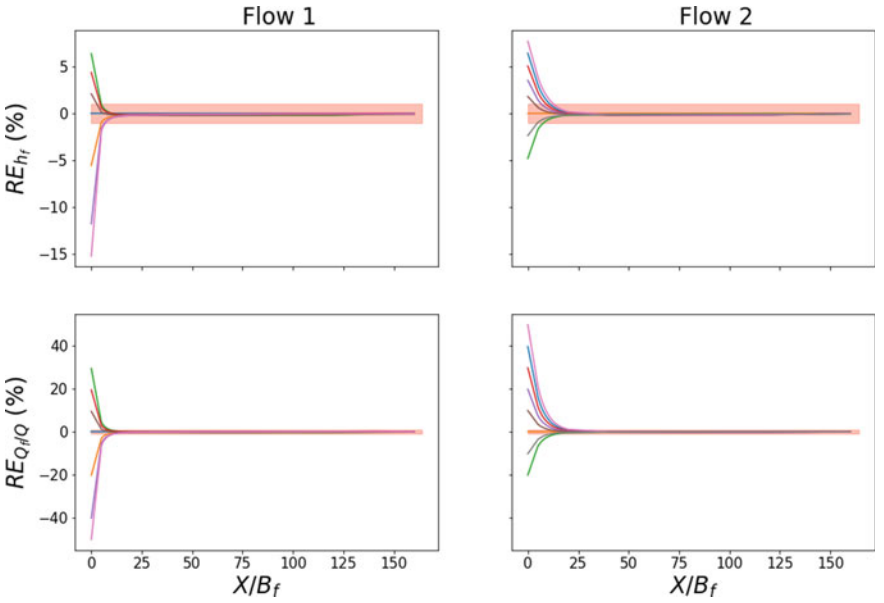

Fig. 5.10 Sensitivity analysis of the inlet discharge distribution in a 167-m-long virtual compound channel. Each color solid line indicates a different inlet discharge partition

are no dykes at the MC/FP interface along the modelled area, which makes relevant the study of overbank flows in a compound channel geometry. The downstream boundary condition was chosen just upstream of the confluence with the channel flowing from the Gervans power-plant outlet.

Because the shallow water equations cannot be solved easily for dry conditions, the ISM modelling suffers from important limitations for inbank flows, which reduces its use for operational purposes. Therefore, two specific water profiles ensuring the complete flooding of the lateral adjacent floodplains (green polygons in Fig. 5.11) were selected. The water levels were picked on 10/03/2001 and on 16/11/2002. During that two events, the discharge was small enough to let the far floodplain completely dry (pink polygons), so that the computational domain restricted to the adjacent floodplains where the flow was only modelled using the shallow water equations. Three numerical codes were benchmarked on this study-case, namely, MAGE-DEBORD (corrected-DCM), MAGE-ISM (ISM) and FudaaCrue (DCM), the operational code from Compagnie Nationale du Rhône (C.N.R) detailed in Rothé et al. [23] (Table 5.3).

The simulations were run with a proper modelling of the selected area, one for MAGE and one for FudaaCrue, since they were already available for each numerical code, ether in INRAE or in CNR. The 2 models relied on the same topographical survey. The bathymetric information was collected in 2006. Nevertheless, the further treatments of the geometry partially differed, resulting in some local differences in the geometry of MAGE and FudaaCrue models (e.g. the floodplain total extent

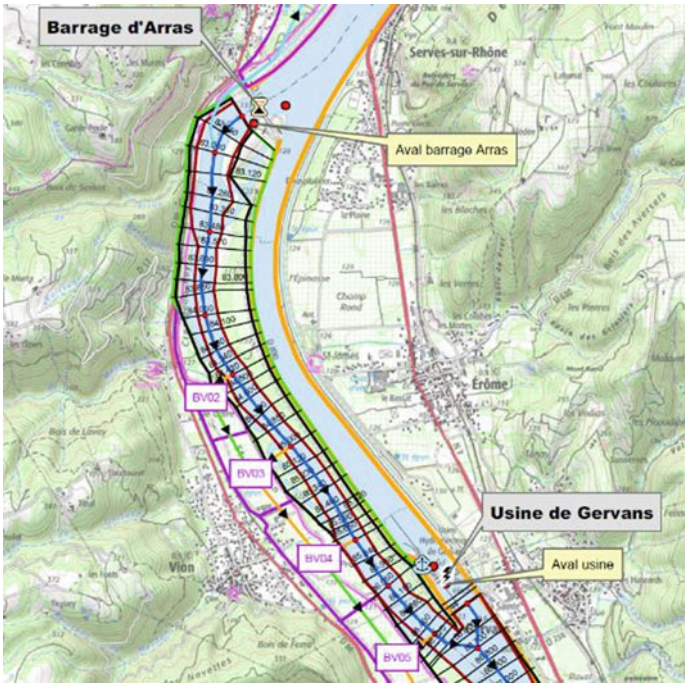

Fig. 5.11 Map of the modelled area, upstream part of the Bourg-Lès-Valence reservoir, Rhône river, France. The black and green polygons limit the computational domain, where the flow is modelled using the shallow water equations. It consists of a main channel (brown polygon) and local adjacent floodplains (green polygons). The far floodplains, depicted here by the pink polygons, were not submerged during the two simulated events. Barrage d'Arras and Usine de Gervans stand for Arras dam and Gervans power plant, respectively

Table 5.3 Main characteristics measured for water level profiles sampled on 10/03/2001 and on 16/11/2002

Water level profiles	$Q\,f\_1$($m^3.s^{-1}$)	Q ($m^3.s^{-1}$)	$Q\,f\_r$($m^3.s^{-1}$)	$Q\,tot$($m^3.s^{-1}$)	Z_{dn}(m. NGF Ortho)
10/03/2001	323	1524	414	2261	121.41
16/11/2002	511	2120	669	3300	121.38

Q_{tot} stands for the inflow discharge dor DCM models. Q_{f_1}, Q_m, Q_{f_r} denote the discharge distribution within the different subsection set in the ISM model as the upstream boundary condition) and Z_{dn} denotes the downstream water level used as downstream boundary conditions in every model

was somehow larger in several FudaaCrue sections). Each of the model was calibrated independently, according to the guidelines and good practices of each institute. FudaaCrue was calibrated on 7 water level profiles obtained for discharges ranging from 60 to 3300 $m^3.s^{-1}$ whereas the discharge ranges from 766 to 3198 $m^3.s^{-1}$ for MAGE-DEBORD calibration. At the time of the model building, the calibration

was performed manually for the two models, since advanced method like the semi-automatic calibration procedure developed by Rothé et al. [23], was not available for FudaaCrue yet. At this step, the correct procedure to calibrate MAGE-ISM for operational purposes remains unclear since: (i) two new parameters (ψ^t and ϕ) come in addition with Strickler coefficients which may affect the calibration methodology and (ii) we face a lack of available field data for calibrating ψ^t and ϕ so that the relevance of the laboratory estimations can not be criticized or evaluated for field applications. As a result, the Strickler coefficients of MAGE-DEBORD were also used in the MAGE-ISM modelling.

It should be noted that Strickler coefficients are considered as calibration parameters in FudaaCrue. Therefore, their calibration only requests longitudinal profiles of measured water levels as input data. The channel is thus splitted into homogeneous area regarding the number of available water level measurements according to the guidelines specified in [27]. On the contrary, in MAGE-DEBORD, Strickler coefficients are supposed to represent the wall friction. Due to the lack of field information, their value were supposed to be uniform on the entire length of the model.

Finally, a sensitivity analysis was performed to measure the influence of the ψ^t-parameter in the simulations. This last step proved that ψ^t plays a role as significant as the Strickler coefficients in the water levels. Therefore, we ran a last simulation with the ψ^t-value of 0.08 which was shown to improve our previous results. This value differs from the one chosen for the previous step of this work (0.03 for laboratory flows, see Table 4) and primarily used for field simulations. It also differs from the literature (0.02, see [18]) but appears to be closer to the EDM value (0.16, see [2]). The main features of the three models are presented in Table 5.4:

The simulations were analysed through the following metrics: the maximum absolute local bias, the mean absolute bias along the channel and the RMSE between the simulated and measured water levels. The results are presented in Fig. 5.12 and Table 5.5. Interestingly, with default values, MAGE-ISM ($\psi^t = 0.03$) performs equally well with the two DCM codes without any specific calibration procedure. For the water profile taken on 16/11/2002, MAGE-ISM led to the smallest mean absolute bias among the three codes. Despite the worst maximum absolute bias is observed with

Table 5.4 Main Characteristics of the modelling of Bourg-Lès-Valence "Vieux-Rhône" for MAGE-DEBORD, MAGE-ISM and FudaaCrue

Code	ΔX_{t_s} (m)	ΔX_m (m)	N_{Ktot}	N_{Keff}	ψ^t	ϕ
Mage-ISM ($\psi^t = 0.03$)	~ 500	50	210	2	0.03	0.3
Mage-ISM ($\psi^t = 0.08$)	~ 500	50	210	2	0.08	0.3
Mage DEBORD	~ 500	50	140	2	–	–
FudaaCrue	50 to 170	50 to 170	89	26	–	–

ΔX_{t_s} stands for the spatial resolution of the topological survey used to build the model, and ΔX_m, for the numerical resolution of the model after interpolation. The number of available freedom degrees for the calibration (total number of available Strickler coefficients) is denoted as N_{Ktot}, whereas N_{Keff} refers to the effective number of degrees of freedom used in the calibration (effective of K-values in use)

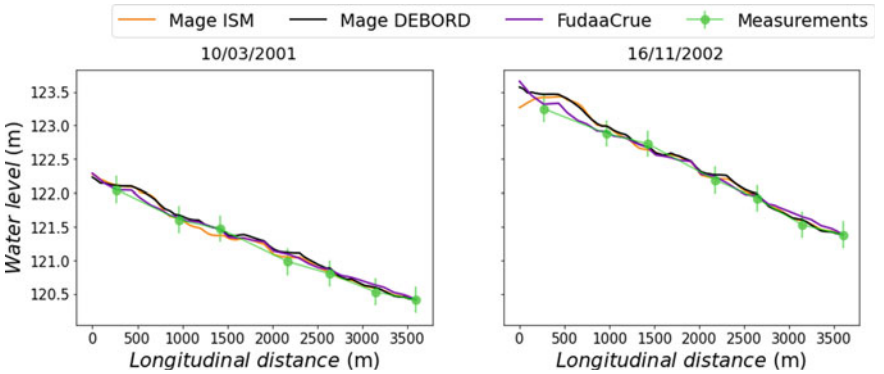

Fig. 5.12 Water level simulations plotted against measurements for two water profiles taken on 10/03/2001 and on 16/11/2002 (MAGE-ISM: $\psi^t = 0.03$)

ISM, resulting from some probable local important gaps, the ISM-RMSE remains limited and shares an acceptable order of magnitude with its two challengers.

Nonetheless, taking into account the possible optimization of the ψ^t –value ($\psi^t = 0.08$), MAGE-ISM appeared to provide better results than any other model, reducing the maximum bias and the RMSE in every simulation.

Considering the mean behavior of the three codes on the two water profiles, whether MAGE-ISM is run with default values, FudaaCrue provides slightly better results despite lower capabilities in the modelling of physical processes. These good performances are explained by the attention paid to the calibration procedure (involving a higher number of freedom degrees) and because the two water level profiles used in the benchmark were also used during the calibration procedure. On the contrary, an optimized value of ψ^t led MAGE-ISM to perform better than any other model in the benchmark. This latter observation proves that the turbulence parameter ψ^t plays a role as significant as the Strickler coefficient in both the physical processes modelling and the calibration.

Such result should be considered as very promising since the more detailed modelling of the different physical processes provided by MAGE-ISM was proven to improve model performances significantly even without proper calibration of the Strickler coefficients. As a result, and despite further confirmations are still needed, MAGE-ISM might be supposed to get more reliable simulations in extrapolation situations, i.e. for discharge conditions out of the calibration range.

Whereas traditional DCM modelling does not allow deriving the discharges in MC and FP, MAGE-DEBORD and MAGE-ISM enable this possibility. Interestingly, the upstream discharge distribution appeared to be very different from MAGE-ISM to MAGE-DEBORD (see Table 5.6). Unfortunately, even if the more precise description of the physical processes in MAGE-ISM let think that the ISM partition is more relevant than the DEBORD's one, no evidence can be afforded yet to prove this latter statement.

Table 5.5 Maximum and mean absolute bias (ε), as well as RMSE of MAGE-ISM (with either $\psi^t = 0.03$ or $\psi^t = 0.08$), MAGE-DEBORD and FudaaCrue simulations of water profiles sampled on 10/03/2001 and 16/11/2002

	10/03/2001			16/11/2002			Mean behavior	
	$Max(\varepsilon(x))$(cm)	$\overline{\varepsilon(x)}$ (cm)	RMSE (cm)	$Max(\varepsilon(x))$(cm)	$\overline{\varepsilon(x)}$ (cm)	RMSE (cm)	$\overline{\varepsilon(x)}$(cm)	RMSE (cm)
MAGE-ISM ($\psi^t = 0.03$)	14.5	6.9	8.5	16.3	4.7	7.1	5.8	7.8
MAGE-ISM ($\psi^t = 0.08$)	**8.5**	5.2	**6.2**	**9.7**	**4.1**	**5.2**	**4.7**	**5.7**
MAGE-DEBORD	12.9	5.9	7.1	7.3	4.9	5.4	5.4	6.3
FudaaCrue	11.1	**4.6**	6.4	11.8	5.1	6.1	4.9	6.2

Table 5.6 Upstream total discharge in the MC right-hand FP and left-hand FP estimated by DEBORD and ISM for the water level profile measured on 10/03/2001

Distribution	Right-hand FP	MC	Left-and FP	Total cross section
Uniform ISM ($m^3.s^{-1}$)	197.79	1816.00	247.21	2261.00
DEBORD ($m^3.s^{-1}$)	322.80	1524.30	413.90	2261.00
Relative difference (%)	38.73	−19.14	40.27	0

The relative difference is computed between DEBORD and uniform ISM

Another simulation was completed after modifications of the MAGE model to take into account the observed differences in the model geometry between MAGE and FudaaCrue. MAGE-DEBORD and MAGE-ISM were thus run over the new geometry including lower spatial resolution and additional sections (totalizing 34 cross-sections) without further calibration. This new computation slighty debased the performances of MAGE-DEBORD leading to an increase of both the mean absolute bias and the RMSE of about 2 cm. The impact on MAGE-ISM was weaker. It was proven that a manual adaptation of the upstream discharge distribution allows maintaining and even improving the performances of MAGE-ISM. Nevertheless, no possibility was offered to compare the adapted distribution to the actual one, since no measurement of discharges in MC and FP were available.

5.5 Conclusions

New numerical and methodological developments of the 1D + ISM model are proposed, in order to make the ISM well suited for operational purposes. They include solver additional developments in order to address unsteady flow conditions, derivation of an upstream boundary condition by partitioning the flow between MC and FPs from routine data, and an additional mass conservation equation for junctions (not tested here).

Some of those developments still rely on basic assumptions such as the approximation of an equivalent steady uniform flow (as in the derivation of the upstream discharge partition between subsections or of the discharge partition at river confluences). Those assumptions are limited and may spoil the ISM performance, particularly when the discharge partition is far from equilibrium, i.e. far from the "equivalent steady uniform flow" partition. This kind of situation should appear in case of flash floods for example.

Those new developments were proved to be relevant against experimental data. First, ISM well captures various transient flow parameters, such as the hysteresis response of the water level to a discharge surge. The behavior of depth-averaged variables at the MC/FP interface, such as the longitudinal and transverse velocity and lateral discharge, are well reproduced in comparison with experimental measurements in a laboratory flume.

The ISM validation against field data also led to satisfactory results, since the RMSE of the observed/simulated water levels remains lower or equal to 10 cm, which is a commonly accepted quality standard by regulatory authorities. Nevertheless, at this stage of development, advanced calibration procedures like the use of meta-heuristic optimization methods still fill the gap and led to similar and even best performance in operational situations.

To conclude, the first steps of ISM improvements for operational purposes led to very promising results, although reliable uses for operational purposes still require further developments (such as improvements in the treatment of junctions as well as in the calibration methodology in order to include the specific parameters ϕ and ψ^t in addition to Manning coefficients). Among the numerous perspectives, we would like to underline the need for solving flows over dry subsections. Further steps also include the derivation of ISM specific equations for hydraulic works (e.g. weirs and juice gates).

Acknonwledgements The Ph.D. of Yassine Kaddi received a financial support from INRAE (Aqua department, 50%) and CNR (Division of innovation and energy supply transition, 50%). The authors are grateful to the help of Fabien Thollet and Alexis Buffet for their assistance during the laboratory measurements.

References

1. Ackers P (1993) Flow formulae for straight two-stage channels. J Hydrau Res 31(4):509–531
2. Bousmar D, Zech Y (1999) Momentum transfer for practical flow computation in compound channels. J Hydrau Eng 125(7):696–796
3. Bousmar D, Wilkin N, Jacquemart JH, Zech Y (2004) Overbank flow in symmetrically narrowing floodplains. J Hydraul Eng 130(4):305–312
4. Bousmar D, Riviere N, Proust S, Paquier A, Morel R, Zech Y (2005) Upstream discharge distribution in compound-channel flumes. J Hydraul Eng 131:408–412
5. Bousmar D, Mathurin B, Fernandes JN, Filonovich M, Hazlewood C, Huthoff F, Leal JB, Paquier A, Proust S (2016) Uniform flow in prismatic compound channel: benchmarking numerical models. River flow 2016, 8th international conference on fluvial Hydraulics. Saint-Louis, Missouri (USA), July 12–15, 2016. G. H. Constantinescu. Taylor & Francis Group, London, pp 272–280
6. Chow VT (1959) Open channel hydraulics, MacGraw-Hill, New-York, p 680
7. Ervine DA, Willets BB, Sellin RHJ, Lorena M (1993) Factors affecting conveyance in meandering compound flows. J Hydraul Eng 119(12):1383–1399
8. Fernandes JN, Leal JB, Cardoso AH (2012) Flow structure in a compound channel with smooth and rough floodplains. Euro Water 38:3–12
9. Huthoff F, Roos PC, Augustjin DCM, Hulscher SJMH (2008) Interacting divided channel method for compound channel flow. J Hydraul Eng ASCE 134(8):1158–1164
10. Kaddi Y, Proust S, Faure JB, Cierco FX (2019) Unsteady flows in a compound open-channel: a laboratory experiment and a 1D+ model. In: E-proceedings of the 38th IAHR World congress. September 1–6, 2019, Panama City, Panama
11. Lai C-J, Liu C-J, Lin Y-Z (2000) Experiments on flood-wave propagation in compound channel. J Hydraul Eng 126(7):492–501
12. Lambert MF, Myers WR (1998) Estimating the discharge capacity in straight compound channels. Proc Inst Civ Eng Water Maritime Energy 20(7):793–801

13. Lilas D, Proust S, Paquier A, Goutal N (2010) Analyse de la pertinence du calage du coefficient de Manning pour des crues faiblement débordantes. SimHydro 2010: hydraulic modeling and uncertainty, 2010, june 2nd–4th, Sophia–Antipolis, France
14. Moretta P, Martin-Vide J (2010) Apparent friction coefficient in straight compound channels. J Hydraul Res 48(2):169–177
15. Nicollet G, Uan M (1979) Ecoulements permanents à surface libre en lits composes. La Houille Blanche 1:21–30. https://doi.org/10.1051/lhb/1979002
16. Peltier Y, Rivière N, Proust S, Mignot E, Paquier A, Shiono K (2013) Estimation of the error on the mean velocity and on the Reynolds stress due to a misoriented ADV probe in the horizontal plane: case of experiments in a compound open-channel. Flow Meas Instrum 34:34–41
17. Proust S, Rivière N, Bousmar D, Paquier A, Zech Y, Morel R (2006) Flow on compound channel with abrupt floodplain contraction. J Hydraul Eng 132(9):958–970
18. Proust S, Bousmar D, Rivière N, Paquier A, Zech Y (2009) Nonuniform flow in compound channel: a 1D method for assessing water level and discharge distribution. Water Resour Res 45:1–16
19. Proust S, Bousmar D, Rivière N, Paquier A, Zech Y (2010) Energy losses in compound open channels. Adv Water Resour 33(1):1–19
20. Proust S, Fernandes JN, Peltier Y, Leal JB, Rivière N, Cardoso AH (2013) Turbulent non-uniform flows in straight compound open-channel. J Hydraul Res 51(6):656–667
21. Proust S, Fernandes JN, Leal JB, Rivière N, Peltier Y (2017) Mixing layer and coherent structures in compound channel flows: effects of transverse flow, velocity ratio and vertical confinement. Water Resour Res 3387–3406
22. Proust S, Nikora VI (2020) Compound open-channel flows: effects of transverse curents on the flow structure. J F M 885:A24. ISSN https://doi.org/10.1017/jfm.2019.973
23. Rothé PL, Cierco FX, Duron L, Balayn P (2018) Meta-heuristic optimization method for the calibration of friction coefficients in 1-D open surface channel modeling. In: Gourbesville P, Cunge J, Caignaert G (eds) Advances in hydroinformatics. Springer Water. Springer, Singapore
24. Takahashi T (1969) Theory of one-dimensional unsteady flows in a prismatic open-channel. Ann Dis Prev Res Inst Kyoto Univ 12B:515–527 (in Japanese)
25. Tominaga A, Nagao M, Mio N, Liu J (1994) Hydraulic characteristics of flood waves passing compound channels. Proc Hydraul Eng 38:443–448
26. Tominaga A, Liu J, Nagao M, Nezu I (1995) Hydraulic characteristics of unsteady flow in open channels with flood plains. Proceeding of the 26th IAHR congress. London, pp 373–378
27. Visse A, Cierco FX, Duron L, Rothé PL, Gressier Y (2020) Validation of a semi-automatically calibrated 1-D open-channel model against experimental data with changes in channel geometry. In: Gourbesville P, Caignaert G (eds) Advances in hydroinformatics. Springer Water. Springer, Singapore. https://doi.org/10.1007/978-981-15-5436-0_77